Sensors and Materials, Vol. 36, No. 1 (2024) 225–233
MYU Tokyo

S & M 3513

Compton Imaging Using Pixelated TlBr Semiconductor Detector

Keitaro Hitomi,[1*] Motohiro Matsumura,[2,5] Kenichi Watanabe,[3]
Shusuke Maruyama,[1,4] Mitsuhiro Nogami,[1] and Uritani Akira[2]

[1]Department of Quantum Science and Energy Engineering, Graduate School of Engineering, Tohoku University, 6-6-01-2, Aza-Aoba, Aramaki, Aoba-ku, Sendai 980-8579, Japan
[2]Department of Applied Energy Engineering, Nagoya University, Furo-cho, Chikusa-ku, Nagoya 464-8603, Japan
[3]Department of Applied Quantum Physics and Nuclear Engineering, Kyushu University, 744 Motooka, Nishi-ku, Fukuoka 819-0395, Japan
[4]Japan Nuclear Fuel Ltd., 4-108 Aza Okizuke, Oaza Obuchi, Rokkasho, Kamikita-gun, Aomori 039-3212, Japan
[5]Toyota Systems Corp., 1-1-1 Meieki, Nakamura-ku, Nagoya 450-6332, Japan

(Received September 28, 2023; accepted January 5, 2024)

Keywords: TlBr semiconductor detector, 3D position sensing, Compton imaging, pixelated detector

Thallium bromide (TlBr) is a candidate material for room-temperature semiconductor gamma-ray detectors with high detection efficiency and energy resolution. By adopting a pixelated detector configuration, a TlBr detector can determine not only the deposition energy but also the 3D positions of interactions between gamma-ray photons and the detector medium. A Compton imager, which can measure the directional distribution of incident gamma rays based on Compton scattering kinetics, can be realized by using the information of deposition energies and interaction positions in the gamma-ray detector. In this study, we demonstrated Compton imaging using a pixelated TlBr semiconductor detector.

1. Introduction

Thallium bromide (TlBr) is a candidate semiconductor material for high-energy-resolution gamma-ray spectrometers.[1–10] Since TlBr has a high effective atomic number (Tl = 81, Br = 35) and high density (7.56 g/cm^3), a TlBr detector has high gamma-ray attenuation ability. Because TlBr also has a relatively wide band-gap energy of 2.68 eV, a TlBr detector can be operated at room temperature. In addition, owing to the improvement of the purification process, recent TlBr crystals have exhibited excellent carrier transport performance.[11] The mobility–lifetime product of electrons in TlBr has been reported to exceed 10^{-3} cm^2/V. As a result, TlBr detectors have shown a high energy resolution of roughly 1% for gamma rays with 662 keV energy.[4,10]

High-performance semiconductor detectors, such as CdZnTe, with 3D position-sensing ability have been applied to gamma-ray imagers using the Compton imaging technique, which is based on Compton scattering kinetics.[12,13] In this technique, positions of gamma-ray interactions, such as Compton scattering and photoelectric absorption, in the detector medium are used to determine the incident gamma-ray direction. TlBr semiconductor detectors with a pixelated detector configuration also have 3D position-sensing ability.[4,10] The lateral positions

*Corresponding author: e-mail: keitaro.hitomi.d4@tohoku.ac.jp
https://doi.org/10.18494/SAM4672

ISSN 0914-4935

of interactions can easily be determined from the anode pixel indicating the signal. There are two possibilities for determining the interaction depth. The first is to use the signal ratio between the cathode and the anode pixel. The induced signals of the anode pixel are hardly affected by the interaction depth because of the small-pixel effect, whereas the signals induced on the planar cathode directly depend on the interaction depth. Consequently, the signal ratio of the cathode to the anode can be an index of the interaction depth. The second possibility is to use the electron migration time, which can be determined from the pulse shape of induced signals. The former possibility is difficult to use to determine multiple interaction positions, whereas the latter is suitable for determining them simultaneously.

The linear attenuation coefficients for Compton scattering for 662 keV gamma rays in semiconductor materials including Si, CdTe, and TlBr are 0.18 , 0.37 , and 0.47 cm^{-1}, respectively. These values were calculated from photon cross section data at NIST XCOM.[14] Since TlBr has the highest linear attenuation coefficient for Compton scattering among them, TlBr is promising for the construction of Compton imagers with high detection efficiency.

In this study, we demonstrate Compton imaging experiments using a fabricated pixelated TlBr semiconductor detector, in which the interaction depth is determined using the electron migration time. We also discuss the strategy for determining the sequential order of interaction points, which is important for estimating the incident gamma-ray direction based on Compton imaging.

2. Materials and Methods

2.1 Pixelated detector

We fabricated a pixelated TlBr semiconductor detector for Compton imaging experiments. The horizontal zone purification process was conducted more than 100 times before crystal growth. To grow the TlBr crystal, the traveling molten zone method was performed. The grown TlBr crystal was cut into a cuboidal shape with dimensions of 6.5 × 6.5 × 5.5 mm^3. Both wide surfaces were polished mechanically, then electrodes were deposited by vacuum evaporation of metal thallium through shadow masks. The device had a monolithic cathode with 5 × 5 mm^2 area and nine pixelated anodes in a 3 × 3 array surrounded by a guard electrode. The area of each anode pixel was 1 × 1 mm^2. Figure 1 shows a photograph of the fabricated pixelated TlBr

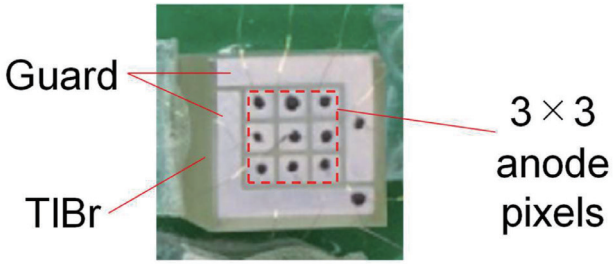

Fig. 1. (Color online) Photograph of the fabricated pixelated TlBr detector.

detector. Finally, the detector was coated with a resin to prevent the deterioration of the Tl electrodes.

Figure 2 shows a block diagram of the signal-processing system. Cathode signals were fed into a digitizer (GaGe, CS8327) through a charge-sensitive preamplifier (Amptek, A250CF). Signals of the pixelated anodes and guard electrode were also digitized using the same digitizer through charge-sensitive preamplifiers (Clear Pulse, CS515-1). The cathode electrode was negatively biased with a voltage of –500 V, while the anodes and guard electrode were grounded. The digitized pulses were recorded by a computer and processed offline.

2.2 Three-dimensional position sensing and depth correction

The fabricated pixelated detector has 3D position-sensing ability. The lateral positions of interactions can be determined from the signals induced by the anodes. In this experiment, the interaction position was estimated to be the center of the anode electrode. Thus, the lateral position resolution was 1.2 mm, corresponding to the pixel width of 1 mm and the interpixel spacing of 0.2 mm. The interaction depth, which is a vertical position between the anode and cathode surfaces, was derived from the electron migration or drift time. Figure 3 shows an example of the induced signals of each electrode for a multiple-hit event. It is difficult to determine the timing of the start of migration because the anode signals are gradually rising owing to the small-pixel effect. Therefore, the start timing of electron migration was determined from the cathode signal. The end timings of migration can be easily determined from each anode signal. In this experiment, the electron mobility was assumed to be the same over the entire crystal. The depth position resolution depended on the accuracy of the estimated electron migration time, which was affected by the signal-to-noise ratio of the detector output signals. Future studies are needed to determine the depth position resolution.

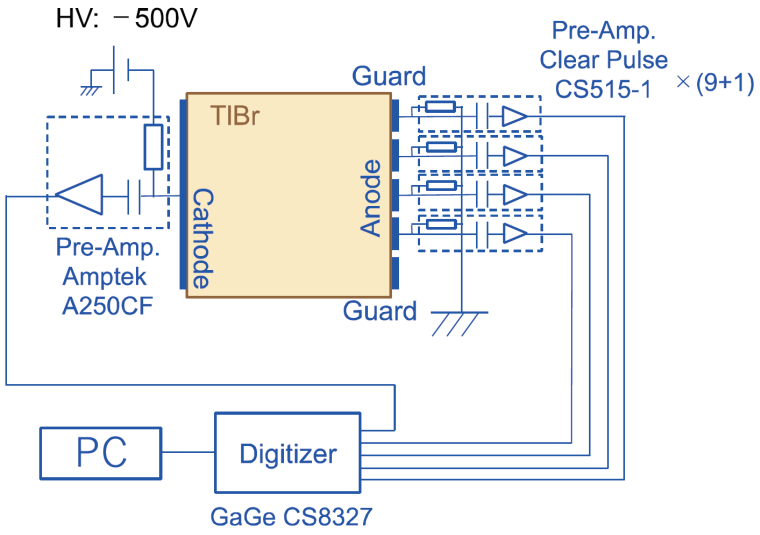

Fig. 2. (Color online) Block diagram of the signal-processing system.

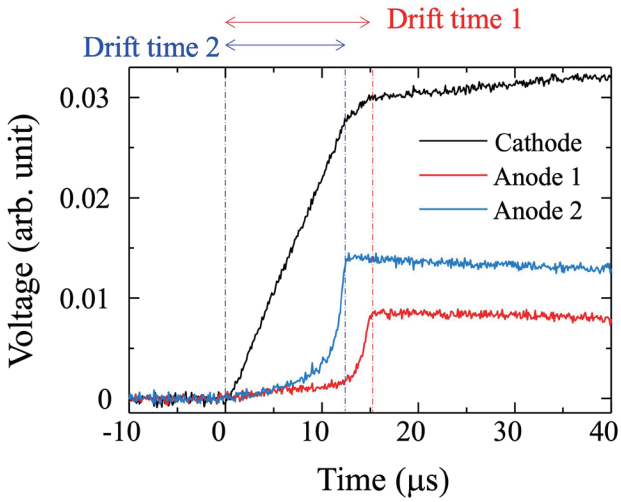

Fig. 3. (Color online) Example of induced signals of each electrode for a multiple-hit event.

The signal pulse height from each anode decreased owing to two factors: carrier decay due to trapping and the incomplete small-pixel effect near anodes. Both factors depend on the interaction depth. However, they have opposite trends. With decreasing distance from the interaction position to the anode surface, the pulse height decreases owing to the incomplete small-pixel effect and it increases without carrier trapping. The carrier decay due to trapping can be derived from the interaction depth using the carrier mobility and lifetime. The incompleteness of the small-pixel effect can also be estimated using the calculated weighting potential in the crystal and the interaction depth. In this experiment, the pulse height was corrected taking into account the interaction depth, the carrier decay due to trapping, and the incomplete small-pixel effect.

2.3 Compton imaging

Compton imaging is based on Compton scattering kinetics. The Compton-scattered gamma-ray photon energy E_γ' is expressed as[15]

$$E_\gamma' = \frac{E_\gamma}{1+\frac{E_\gamma}{m_e c^2}(1-\cos\theta)}, \tag{1}$$

where E_γ is the incident photon energy, θ is the scattering angle, m_e is the electron mass, and c is the velocity of light. According to this equation, the scattering angle can be derived from the incident and Compton-scattered photon energies. If a scattered photon is photoelectrically absorbed in the detector medium, its energy can be determined. When a double-hit event, in

which an incident photon is first scattered and then absorbed, occurs in the detector medium, the incident photon direction is confined within the Compton cone, as described later. As described above, the scattered photon energy is determined from the deposition energy at the final absorption point. The incident photon energy is the total deposition energy at the initial scattering and final absorption points, assuming that the incident photon is fully absorbed without escaping from the detector volume. The Compton scattering angle can be calculated from these energies. The direction of a Compton-scattered photon is derived from the initial scattering and final absorption points. Consequently, the incident photon direction is confined within the Compton cone, the vertex of which is at the initial scattering point, its central axis is defined by line segment between the scattering and absorption points, and its opening angle is equal to the Compton scattering angle. The directional distribution of incident gamma rays can be estimated by superimposing the Compton cones on the projection screen.

2.4 Experimental setup

We performed position estimation experiments using point gamma-ray sources. Figure 4 shows the geometry used in the experiments. The cathode center of the pixelated TlBr detector was placed at the origin. The z-axis was defined as facing the anode side. Positions 1 and 2 were set to $(x, y, z) = (0, 0, 15)$ and $(15, 0, 15)$, respectively, where the unit is mm, so that the positions were on the same plane. We conducted two experiments: a single-source experiment and a double-source experiment. In the single-source experiment, a Cs-137 source emitting 662 keV gamma rays was used. The experiment was conducted for two cases, with the source placed at positions 1 and 2. In the double-source experiment, Cs-137 and Co-60 sources were simultaneously used. The Co-60 source emitted 1.17 and 1.33 MeV gamma rays. The Co-60 and Cs-137 sources were placed at positions 1 and 2, respectively.

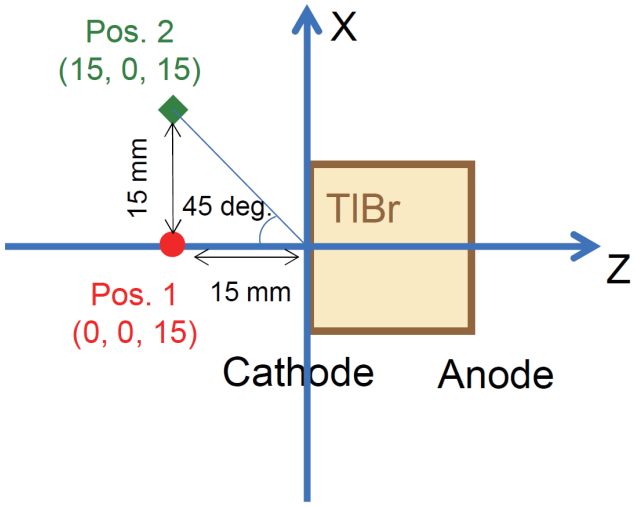

Fig. 4. (Color online) Geometry used in the experiments. The gamma-ray sources were placed on the *x*-*z* plane.

3. Results and Discussion

3.1 Consideration of order of interaction points

As described above, the Compton cone can be determined from the interaction positions and deposition energies at the initial scattering and final absorption points. In the case of double-hit events, there are two interaction points. The remaining issue is how to determine their sequential order. Using the Monte Carlo simulation code EGS5,[16] we calculated the dependence of the probability of double-hit events occurring on the scattering angle in the TlBr detector with a size of 5 × 5 × 5 mm^3 when irradiating 662 keV gamma rays, as shown in Fig. 5. According to the Klein–Nishina formula, which represents the angular distribution of the scattered photons, small-angle scattering is preferential for 662 keV gamma rays.[15] However, double-hit events preferentially occur for a large scattering angle in a relatively small detector. This is because a scattered gamma ray with a large scattering angle has low energy and a short attenuation length. Consequently, events having a scattering angle of more than 90° occur preferentially. In these events, the deposition energy at the scattering point is higher than the scattered gamma-ray energy or the deposition energy at the absorption point. Although there is a slight difference between the simulated and fabricated detector sizes, this feature is applicable to both detectors. Therefore, we adopted the strategy of considering the interaction point with the higher deposition energy as the scattering point.

However, according to Eq. (1), the scattered gamma ray has the minimum energy when it is scattered directly backward. In other words, the deposition energy at the scattering point has the maximum value, which is well known as the Compton edge energy. If the deposition energy at an interaction point exceeds the maximum value, the point is considered as the absorption point.

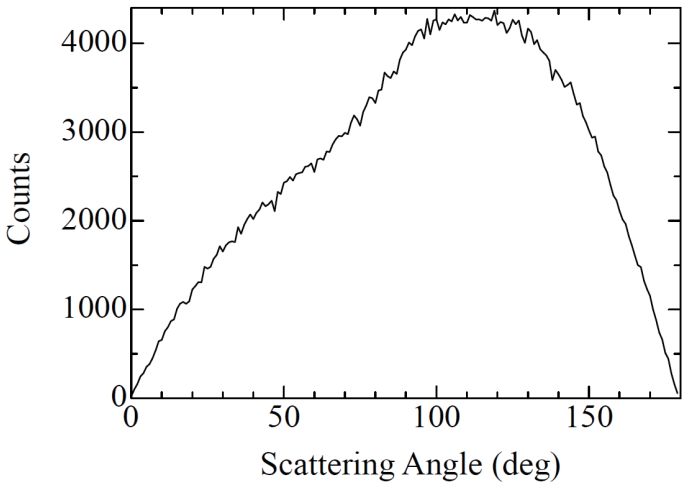

Fig. 5. Dependence of the probability of double-hit events occurring on the scattering angle in the TlBr detector with a size of 5 × 5 × 5 mm^3 when irradiating 662 keV gamma rays.

We confirmed the validity of this strategy for determining the order of interaction points through a Monte Carlo simulation study. For incident 662 keV gamma rays, we correctly estimated the order using this strategy in more than 80% of the events.

3.2 Estimation of source direction

First, we estimated the directional distribution of the incident gamma rays in the single-source experiments. Figure 6 shows the estimated directional distribution of the incident gamma rays at source positions 1 and 2. Only events with a total deposition energy of 662 keV ± 5% were used to create the map. The directional map was drawn using the Mercator projection. The gamma-ray intensity profiles on the equator are also shown in Fig. 6(c). Source position 2 corresponds to a latitude of 45°, as shown in Fig. 4. We successfully demonstrated that the estimated source positions agreed with the actual ones.

Additionally, we estimated the directional distribution of the incident gamma rays in the double-source experiment. In this case, for the estimation of the Co-60 source, we used events with total deposition energies of 1.17 MeV ± 10% and 1.33 MeV ± 10%. The data were acquired

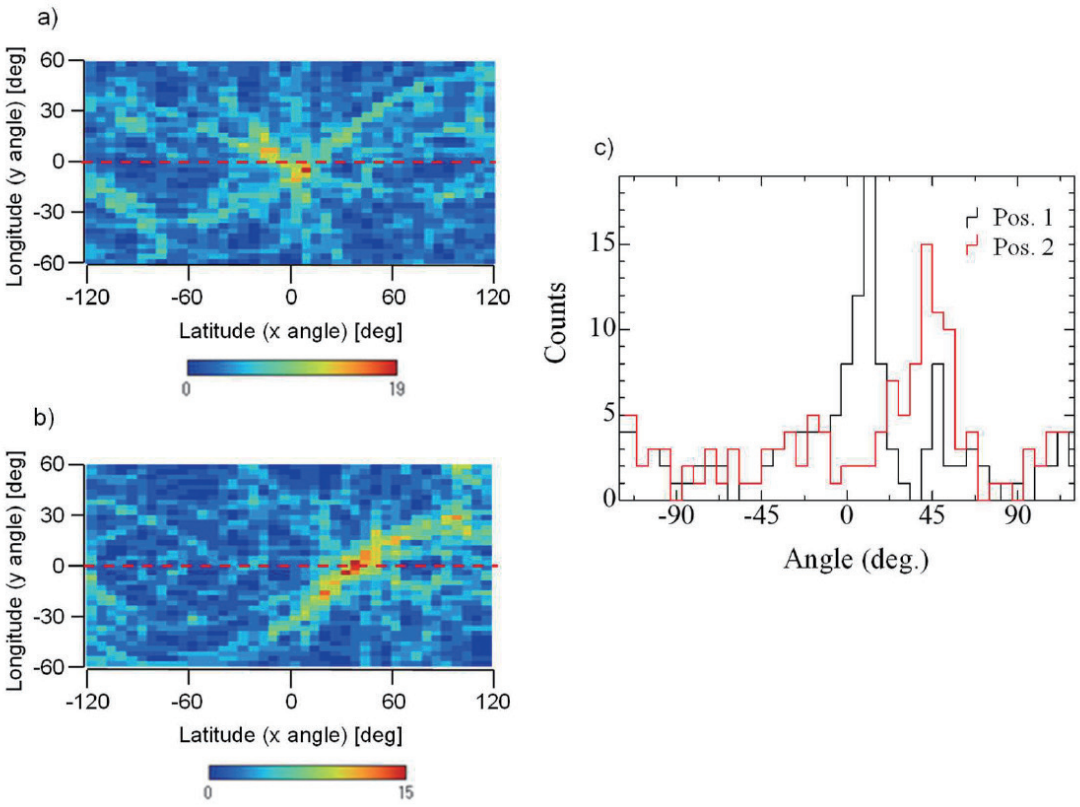

Fig. 6. (Color online) Estimated directional distribution of incident gamma rays at (a) source position 1 and (b) source position 2 in the single-source experiments. (c) Gamma-ray intensity profiles on the equator of (a) and (b) (red dashed line).

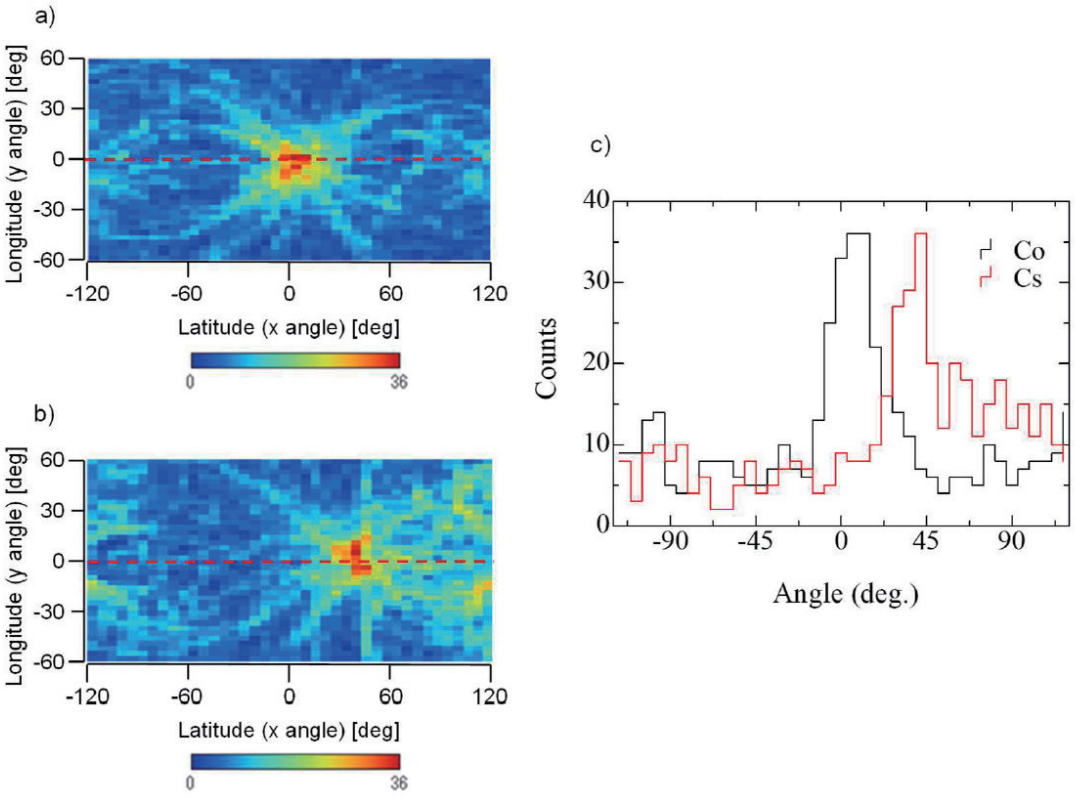

Fig. 7. (Color online) Estimated directional distribution of the incident gamma rays for (a) Co-60 and (b) Cs-137 sources in the double-source experiment. (c) Gamma-ray intensity profiles on the equator of (a) and (b) (red dashed line).

for the situation that the Cs-137 and Co-60 sources were simultaneously placed at the different points. Figure 7 shows the estimated directional distribution of the incident gamma rays for the Co-60 and Cs-137 sources in the double-source experiment. The gamma-ray intensity profiles on the equator are also shown. We confirmed that the positions of the sources emitting gamma rays with different energies can be separately estimated.

However, the obtained images were distorted mainly due to the insufficient number of pixels in the detector, which limited the angle of the Compton cone. To improve the image quality, it is necessary to increase the number of pixels and improve the imaging algorithm.

4. Conclusions

We performed Compton imaging experiments using a pixelated TlBr semiconductor detector. This detector can determine the deposition energies and 3D positions of interaction points between a gamma-ray photon and the detector medium. To simultaneously estimate interaction points in multiple-hit events, the electron migration length or time is beneficial. When using a

relatively small detector for Compton imaging, the strategy of considering the interaction point with the higher deposition energy as the scattering point is preferred. By adopting this strategy and considering the maximum deposition energy at the scattering point, the correct order of interaction points was predicted in more than 80% of the events under 662 keV gamma-ray irradiation. Finally, we successfully demonstrated that the source positions estimated by the fabricated Compton imager agreed with the actual ones, even for two sources with different energies.

References

1 K. Hitomi, T. Murayama, T. Shoji, T. Suehiro, and Y. Hiratate: Nucl. Instrum. Methods Phys. Res., Sect. A **428** (1999) 372. https://doi.org/10.1016/S0168-9002(99)00141-2
2 K. Hitomi, O. Muroi, T. Shoji, T. Suehiro, and Y. Hiratate: Nucl. Instrum. Methods Phys. Res., Sect. A **436** (1999) 160. https://doi.org/10.1016/S0168-9002(99)00614-2
3 T. Onodera, K. Hitomi, T. Shoji, and Y. Hiratate: Nucl. Instrum. Methods Phys. Res., Sect. A **525** (2004) 199. https://doi.org/10.1016/j.nima.2004.03.046
4 K. Hitomi, T. Onodera, T. Shoji, and Z. He: Nucl. Instrum. Methods Phys. Res., Sect. A **578** (2007) 235. https://doi.org/10.1016/j.nima.2007.05.113
5 K. Hitomi, T. Shoji, and Y. Niizeki: Nucl. Instrum. Methods Phys. Res., Sect. A **585** (2008) 102. https://doi.org/10.1016/j.nima.2007.11.012
6 K. Hitomi, Y. Kikuchi, T. Shoji, and K. Ishii: Nucl. Instrum. Methods Phys. Res., Sect. A **607** (2009) 112. https://doi.org/10.1016/j.nima.2009.03.129
7 B. Dönmez, Z. He, H. Kim, L. J. Cirignano, and K. S. Shah: Nucl. Instrum. Methods Phys. Res., Sect. A **623** (2010) 1024. https://doi.org/10.1016/j.nima.2010.08.024
8 K. Hitomi, T. Shoji, and K. Ishii: J. Cryst. Growth **379** (2013) 93. https://doi.org/10.1016/j.jcrysgro.2013.03.002
9 K. Hitomi, T. Tada, T. Onodera, S.-Y. Kim, Y. Xu, T. Shoji, and K. Ishii: IEEE Trans. Nucl. Sci. **60** (2013) 1156. https://doi.org/10.1109/TNS.2012.2217155
10 K. Hitomi, T. Onodera, S-Y. Kim, T. Shoji, and K. Ishii: Nucl. Instrum. Methods Phys. Res., Sect. A **747** (2014) 7. https://doi.org/10.1016/j.nima.2014.02.020
11 K. Hitomi, T. Onodera, and T. Shoji: Nucl. Instrum. Methods Phys. Res., Sect. A **579** (2007) 153. https://doi.org/10.1016/j.nima.2007.04.028
12 D. Xu, Z. He, C. E. Lehner, and F. Zhang: Proc. SPIE 5540, Hard X-Ray and Gamma-Ray Detector Physics VI (2004). https://doi.org/10.1117/12.563905
13 C. G. Wahl, W. R. Kaye, W. Wang, F. Zhang, J. M. Jaworski, A. King, Y. A. Boucher, and Z. He: Nucl. Instrum. Methods Phys. Res., Sect. A **784** (2015) 377. https://doi.org/10.1016/j.nima.2014.12.110
14 M. J. Berger, J. H. Hubbell, S. M. Seltzer, J. Chang, J. S. Coursey, R. Sukumar, D. S. Zucker, and K. Olsen: XCOM: Photon Cross Section Database, National Institute of Standards and Technology (2010). https://dx.doi.org/10.18434/T48G6X
15 G. F. Knoll: Radiation Detection and Measurement (Wiley, New York, 2010) 4th ed., Chap. 2.
16 H. Hirayama, Y. Namito, A. F. Bielajew, S. J. Wilderman, and W. R. Nelson: KEK Report 2005-8 (2005).